



Experimental Setup of an Innovative Multi-Axle Roller Rig for the Investigation of the Adhesion Recovery Phenomenon

N. Bosso¹ · A. Gugliotta¹ · M. Magelli¹ · N. Zampieri¹

Received: 13 February 2019 / Accepted: 12 May 2019 / Published online: 23 May 2019
© The Society for Experimental Mechanics, Inc 2019

Abstract

Proper values of the adhesion coefficient are the key to guarantee good operations of railway transportation systems in terms of safety, performances and punctuality during both braking and traction manoeuvres. Adhesion can drop to very low values due to contaminants lying on the track. However, the leading wheelsets have a cleaning effect on the rail, so that adhesion recovery can be observed on the following axles. A good knowledge of adhesion and adhesion recovery phenomenon is thus fundamental to optimize the dynamic behaviour of railway vehicles and to develop new algorithms for wheel slide protection (WSP) and antiskid systems. Several laboratory facilities are used to investigate adhesion, due to the high costs of on-track tests with full vehicles. Anyway, these devices do not allow a good simulation of the vehicle dynamics and of the real contact conditions. To overcome these issues, roller rigs usually represent a good compromise in terms of costs, safety, repeatability of the tests and simulation of the real contact conditions and vehicle dynamics. However, typical roller rigs consist of one or more wheelsets rolling over separate pair of rollers. An evolution of roller rigs, consisting of multiple wheelsets acting on the same contaminated surfaces, is thus needed to study the adhesion recovery phenomenon more properly. The paper concerns the experimental setup of an innovative 1:5 scaled multi-axle roller rig developed at Politecnico di Torino. The rig is intended to allow researchers to obtain a deep understanding of the mutual interaction of different following wheelsets running on a contaminated track.

Keywords Adhesion · Adhesion recovery · Roller rig · Wheel-rail contact · Friction

List of Symbols

Latin Alphabet

f	Adhesion coefficient
F_b	Braking force
F_s	Suspension load
F_x	Tangential load at the wheel-roller interface
g	Gravity acceleration
$I_{R,yy}$	Polar inertia of the rollers
$I_{w,yy}$	Polar inertia of the wheelset
m	Mass of the wheelset
N	Normal load at the wheel/roller interface
p_{FVB}	F _b pressure at the outlet of the valves
p_{SET}	Set pressure at the outlet of the valves
R_{PAD}	Braking effective radius
R_R	Roller radius
R_w	Wheel radius

T_M	Torque produced by the motor
$T_{R,0}$	Initial resistant torque
$T_{R,b}$	Resistant torque due to braking effort
V_{IN}	Set voltage
V_{OUT}	FeedBack voltage

Greek Alphabet

α	Angle of inclination of the wheelset
ξ	Creep
τ	Transmission ratio (ration between roller and wheel radius)
ω_R	Angular speed of the rollers
ω_w	Angular speed of the wheels
$\dot{\omega}_R$	Angular acceleration of the rollers
$\dot{\omega}_w$	Angular acceleration of the wheelset

Subscripts

b	Braking
i	Wheelset number ($i = 1 \div 4$)
j	Wheel number ($j = 1,2$)
R	Roller
s	Suspension
w	Wheelset

✉ N. Zampieri
nicolo.zampieri@polito.it

¹ Politecnico di Torino, Department of Mechanical and Aerospace Engineering, C.so Duca degli Abruzzi 24, 10129 Torino, Italy

Introduction

The adhesion coefficient is a critical aspect for the operation of railway transportation systems in terms of safety, performances and punctuality during both braking and traction manoeuvres. Many contaminants, such as water, oil, grease, leaves and snow can lie on the wheel-rail interface, causing a drop in the adhesion level. Sand can be spread onto the rails to restore dry adhesion conditions, whereas friction modifiers are used to keep adhesion at a constant optimum level. Since all these substances can be found between the wheel and the rail, it is of great importance to know how they affect adhesion, in order to improve the running behaviour of railway vehicles.

On-track tests can be performed to study adhesion, either with vehicles under operating conditions [1] or with proper instrumentation, such as hand-pushed tribometers [1] and pendulum rigs [2]. On-track tests with full vehicles are difficult to perform due to high costs, safety issues, line occupation and the need of the vehicle itself. Thus, they are not a suitable solution for vehicles during the early stages of design. Moreover, tests conditions cannot be reproduced with enough repeatability. On the other hand, tests with hand-pushed tribometers and pendulum rigs are less expensive, but they do not allow the simulation of the real vehicle dynamics and contact geometry, so they cannot provide useful data to develop adhesion algorithms.

To overcome the issues related to high costs and repeatability, several devices are used for laboratory investigation of adhesion conditions, such as pin-on-disc machines [3, 4], mini-traction machines [5, 6], twin-disc machines [7–11] and scaled [12–16] or full-scale [17–19] roller rigs.

Pin-on-disc machines consist of a pin sliding over a rotating disc. These devices simulate pure sliding motion, without considering the rolling effect, so they do not represent the typical real contact conditions, where the contact area is both in adhesion and slip.

Mini-traction machines are similar to pin-on-discs, but they allow the reproduction of rolling-sliding relative motion thanks to a rolling ball (sample), pressed against the rotating disc. This configuration allows to consider an additional degree of freedom (d.o.f) to the sample with respect to the traditional pin-on disc devices. These facilities can be used to obtain both adhesion and Stribeck curves, by varying the speed of the disc.

In twin-disc machines, two discs, usually made of the same materials of wheels and rails, are pressed against each other. By controlling the speed of both discs, it is possible to reproduce different creep values and to obtain adhesion characteristics, both for dry and contaminated conditions.

The main drawbacks related to pin-on-discs, mini-traction machines and twin-discs are that they do not manage to represent the dynamic behaviour of railway vehicles and that they do not simulate the real contact geometry. Therefore, these

facilities are used to characterize the materials from a tribological and frictional point of view, both for dry and contaminated conditions.

Researchers make use of roller rigs to obtain a better reproduction of the kinematics of the vehicle, as these devices are intended to simulate the real interaction among contact geometry, dynamics and forces acting on the wheel-rail interface. Roller rigs are based on the replacement of the track with rotating rollers, and they are used to study railway vehicle dynamics, wheel-rail contact and to validate numerical and analytical models [20]. Full-scale roller rigs allow a direct comparison with the real case of a vehicle running along a tangent track, while scaled roller rigs require similitude models [21–23]. However, scaled rigs are less expensive and less cumbersome and thus they are largely used to investigate adhesion conditions. Both full-scale and scaled roller rigs differ from the real conditions of vehicle and track due to these five main aspects [18]:

- 1) Alteration of the longitudinal creepage as the rolling radius of the rollers changes when the contact point is shifted along the lateral direction;
- 2) Alteration of the spin creepage due to the normal component of the roller angular velocity;
- 3) Curvature of the rollers in the longitudinal direction;
- 4) Presence of both yaw and pitch angles when the wheelsets yaw over the rollers;
- 5) Different stiffness between the real track and the rollers.

Therefore, many authors have suggested methods to obtain a correlation between the results obtained with roller rigs and the real wheel-rail case [24, 25].

Related to degraded adhesion conditions is the adhesion recovery phenomenon. In fact, when a vehicle is running along a contaminated track, the leading wheelsets have a cleaning effect on the rails, so that dry adhesion levels can be restored on the following ones. Adhesion recovery is normally used to describe the improvement of the adhesion conditions due to large creep values. Normally this phenomenon is related to a single wheelset that can experience an increase in the friction coefficient when the work of the friction forces is able to remove or destroy some of the contaminant. In this case the phenomenon should be defined as wheel adhesion recovery. The paper describes the improvement of adhesion conditions due to the mutual interaction of different following wheelsets running on a contaminated track. In this case still the work of the friction forces removes the contaminant, modifying the adhesion condition, but in a specific track section. This phenomenon should be defined as rail adhesion recovery. Since both phenomena are related to the work of friction forces the term adhesion recovery is used in the paper for the sake of clarity. Modern railway vehicles are equipped with mechatronic devices, such as wheel slide protection (WSP) [26–28] and anti-skid [29, 30] systems. Therefore, a deep understanding of

adhesion recovery is crucial to develop new efficient algorithms for these facilities and to improve the performance and the safety of the vehicle during braking and traction operations.

Twin-disc machines have been used to assess the retentivity of different types of grease [31], but also to investigate the recovery time needed to restore a stable value of adhesion coefficient after the application of sand [10, 32] and water-based friction modifiers [33–35] onto the interface. Similar experiments were performed by Galas et al. [6] with a mini-traction machine, assessing the performance of oil-based friction modifiers. However, since both twin-disc and mini-traction machines are made up of a single pair of bodies pressed against each other and do not allow a proper simulation of the dynamic behaviour, these experimental devices are not suitable for the investigation of the adhesion recovery phenomenon.

Voltr and Lata [36] studied adhesion recovery with a single wheel test rig and provided an analytical model based on the data acquired during several series of experimental tests. Allotta et al. [37, 38] suggested an innovative HIL approach to study adhesion recovery: the software part includes a multibody model of the UIC-Z1 coach, a control block and a degraded adhesion model, whereas the hardware part is represented by the four axles full-scale roller rig in Osmannoro (Florence).

Bosso and Zampieri [39] studied adhesion recovery with a single wheelset scaled roller rig, making use of a probe, covered with a porous tissue to apply contaminants over the surface of the roller, and of a cleaning system. The last one was used to clean the wheel surface and to simulate the contact of a new wheelset at each rotation of the roller. Anyway, the inefficiencies of the cleaning system could lead to a difficult interpretation of the results obtained with this configuration. This experimental activity hence pointed out that adhesion recovery investigation requires multiple wheels rolling over the same surface. The authors have thus designed an innovative multi-axle roller rig [40] (see Fig. 1), which is able to

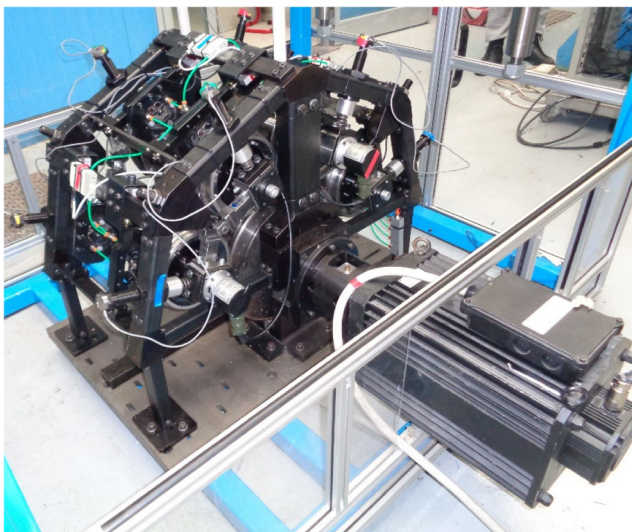


Fig. 1 PoliTo multi-axle roller rig

simulate the mutual interaction among four following wheelsets rolling over the same pair of rollers. The typical operating conditions which can be simulated with the test bench are shown in Table 1. The design of this test rig is carefully described in the first part of the paper, which also shows the control strategy and the acquisition of the signals provided by the measuring instruments installed on the test bench. Finally, the calibration procedure of the sensors and some experimental results (i.e., adhesion characteristics) are presented in the second part of this work.

Multi-Axle Roller Rig Design

The multi-axle roller rig is a 1:5 scaled roller rig following Jaschinski's similitude model [21]. As shown in Fig. 2, each wheelset is arranged over the rollers at a certain angle of inclination α_i to optimize the size of the rig and to maximize the radial component of gravity.

The multi-axle roller rig is derived from the single wheelset [14, 39] test bench and it is designed in order to fit on the same pair of rollers. In this way it is still possible to maintain the modularity that characterizes the test benches realized by the research group of the Politecnico di Torino.

The rig consists of 5 main modules:

- 1) Frame;
- 2) Rollers;
- 3) Wheelsets;
- 4) Braking system;
- 5) Suspension system.

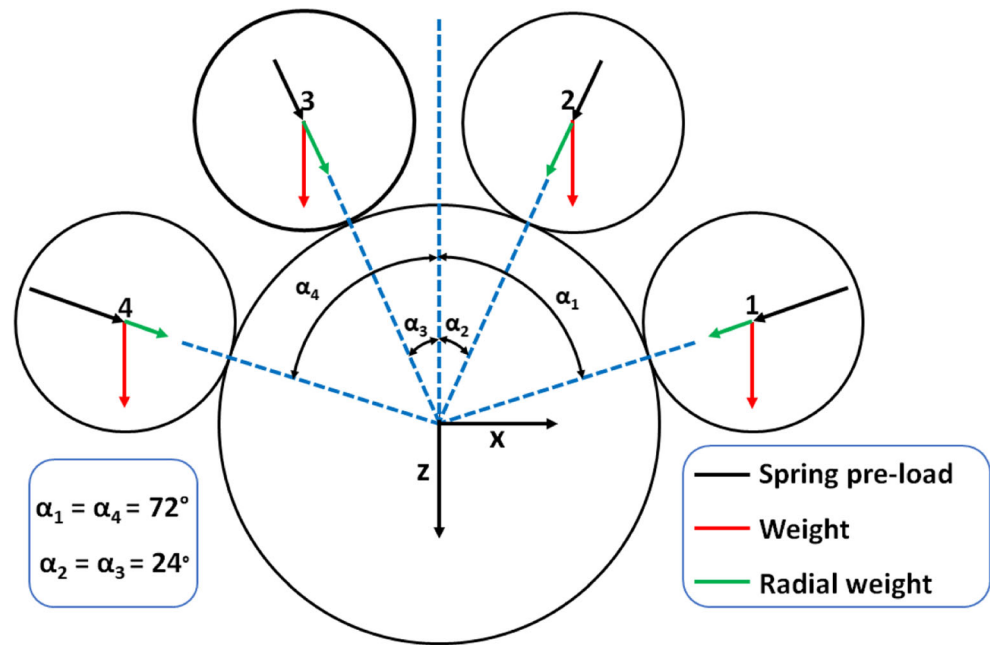
The frame is made up of S235 cold-rolled steel profiles and properly designed mechanical fittings in order to ease the installation of the rig on the base.

Each roller is mounted on a separate support (2), see Fig. 3, to allow an independent drive and the simulation of different values of the railway gauge. However, during the experimental activity shown in this article, the rollers were coupled with a mechanical joint and only one 6 poles brushless AC Motor (ACM BRL 220 6) was used to power the system. The roller profiles (4) are produced by machining a 39NiCrMo6 steel

Table 1 Typical operating conditions that can be simulated with PoliTo multi-axle roller rig

Name	Symbol	Value
Wheel radius	R_w	460–520 mm
Roller radius	R_R	184–208 mm
Axle-load	Q	2–25 ton
Train speed	v	4–310 km/h
Railway gauge	$2s$	1435/1524/1667 mm

Fig. 2 Arrangement of the wheelsets over the rollers



rim, which is fastened with bolts to the disc (5). The diameter of the mounted roller is equal to 368 mm. The surface of the rim reproduces a 1:5 scaled UIC-60 profile, canted 1:20. This solution is used in order to replace only the rim in case of severe wear of the surfaces or in case of the testing of new rail profiles.

Each of the four wheelsets, see Fig. 4, consists of a shaft (1), two wheels, two axle-boxes (4) and two brake discs (6). The wheels, with a radius equals to 184 mm, are made up of a 39NiCrMo3 steel rim (2), reproducing a 1:5 scaled S1002 profile, and a hub (3) connected to the shaft with a parallel key joint (7). Bolts (10)

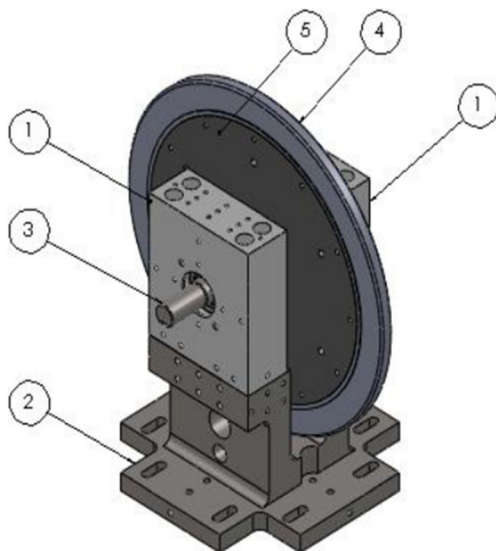


Fig. 3 PoliTo multi-axle roller rig: single roller

connect each wheel-brake disc to a brake drum (8). The axial position of the wheels and the discs is assured by a lock nut (5) tightened on the shaft. Mechanical brackets (9) mounted on the axle-box connect the wheelsets to the frame. These brackets can be regulated in order to ensure that the force of the spring is always in radial direction, also when different wheel or roller diameters are considered.

The braking system, shown in Fig. 5, is based on two brake calipers (Brembo P32G) mounted on each wheelset and supplied with compressed air. The module is fixed to the main frame by two parallel bars (6 and 7). Each caliper (1) is fixed to a plate (2) integral with the bracket (3). The last one is locked in longitudinal direction by the load cell (4), while in the opposite side it is free to translate, but the rotation is prevented by the anti-rotation device (5). This configuration assures that the braking force can be measured by the load cell. Graphite bushings (8) are used in order to allow a frictionless sliding between the caliper brackets and the supports.

Each axle-box is equipped with a suspension system, shown in Fig. 6, which applies a normal contact force to the wheel-roller interface. The system is composed by a hex-head threaded pin (1) which moves in radial direction with respect to the threaded element (7) and presses the spring holder (3). The nut (8) is used to fix the threaded element (7) to the external frame (2). In order to measure the force generated by the spring (4) the pin (5) slides inside the hex-head threaded pin transferring the load to the button cell (6). The system permits the simulation of different values of axle-

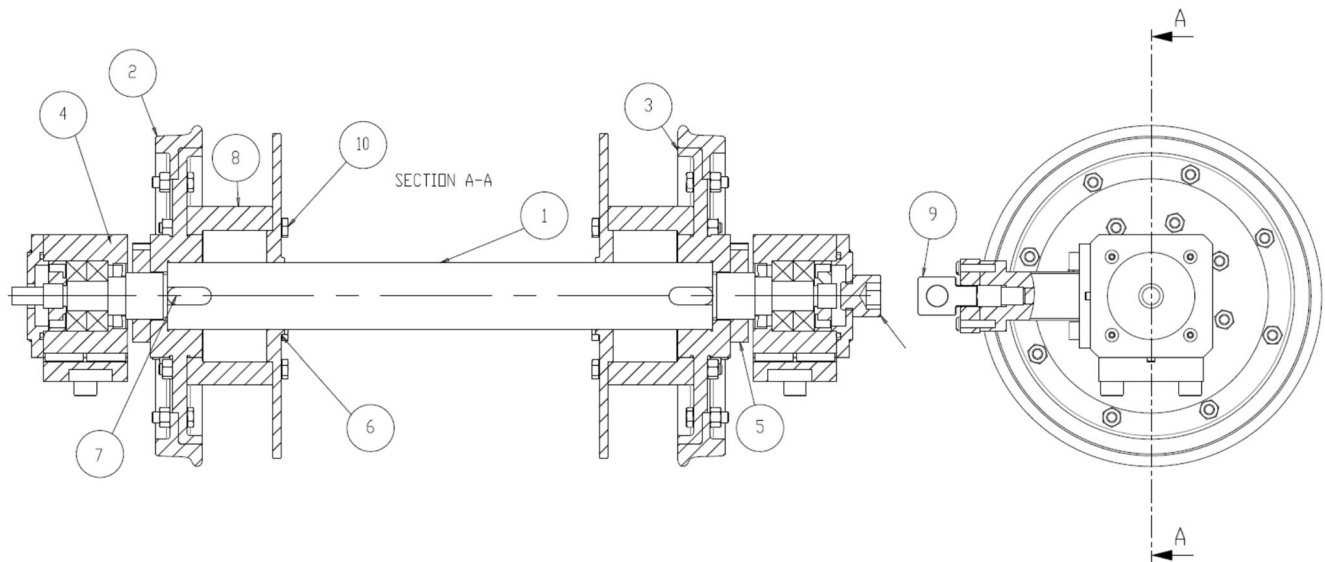


Fig. 4 PoliTO multi-axle roller rig: section view of the wheelset

loads, in order to reproduce several contact conditions for both freight and passenger vehicles. The suspension system allows to consider only the vertical behaviour of the wheelset since the brackets are rigid in longitudinal and lateral directions. The test bench is hence able to simulate only the longitudinal behaviour of the vehicle, which is normally sufficient to simulate braking and traction operations. Furthermore, this configuration allows to obtain better values of repeatability in the experimental results. The suspension system allows to independently regulate the lateral position of each wheelset before running the experimental tests. In future works the suspension system could be modified in order to consider the lateral behaviour of the vehicle, which can affect the adhesion conditions especially for high speed values.

Control and Data Acquisition Strategy

The test bench is controlled by an industrial PC (NI PXIe-8840 quad core processor installed on NI PXI-1050 chassis), produced by National Instruments and running the LabVIEW 2016 software. The schematic view of the acquisition and control strategy is shown in Fig. 7. The real-time controller allows to acquire the signals generated by the sensors and to control the motor and the caliper braking pressure. The communication between the controller and the drives is performed by the TCP-IP Modbus protocol. The sensors, see Table 2, installed on the roller-rig allow to calculate the wheel-rail adhesion coefficient:

Fig. 5 PoliTo multi-axle roller rig: section view of braking system

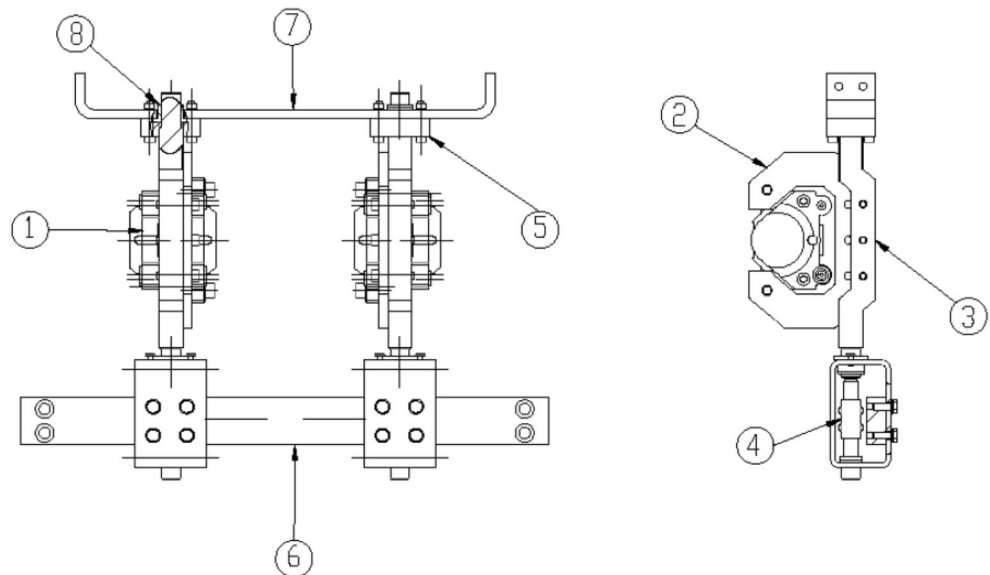
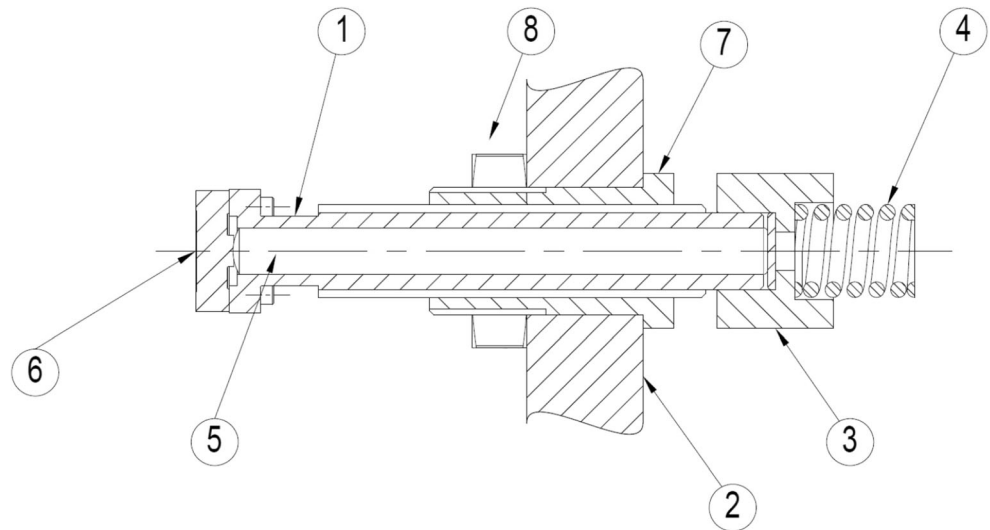


Fig. 6 PoliTo multi-axe roller rig: section view of the suspension system



- 4 incremental single ended encoders (ELAP REM470–1024-8/24-R-10-PP2) with resolution of 10 bit (1024 pulses per revolution) to measure the angular speed of each wheelset. The signals generated by the encoders are acquired by means of the PXIe-6612 counter/timer module that allows a maximum sampling frequency of 1 kHz.
- 8 full bridge load button cells (FUTEK LLB 400 FSH 00877), mounted on the suspension systems, with a maximum load of 1000 lb. (453.6 kg) and resolution of 0.5 lb. (0.27 kg), and 8 full bridge S-beam load cells (FUTEK LSB 302 FSH 02089), with a maximum load of 300 lb. (136.1 kg) and resolution of 0.15 lb. (0.068 kg), installed

on the braking system to measure the braking effort. The signals generated by all the load cells are acquired using two strain-bridge input modules NI PXIe-4330 that allow a maximum sampling frequency of 25.6 kS/s.

The angular speed of the rollers is instead directly obtained from the motor drives by means of the Modbus protocol. The braking pressure, on each couple of calipers mounted on the wheelset, is controlled by four compact electro-pneumatic regulators SMC ITV-0050 3BS, that can set the outlet pressure in the range 0 ÷ 9 bar. The regulators are voltage-controlled in

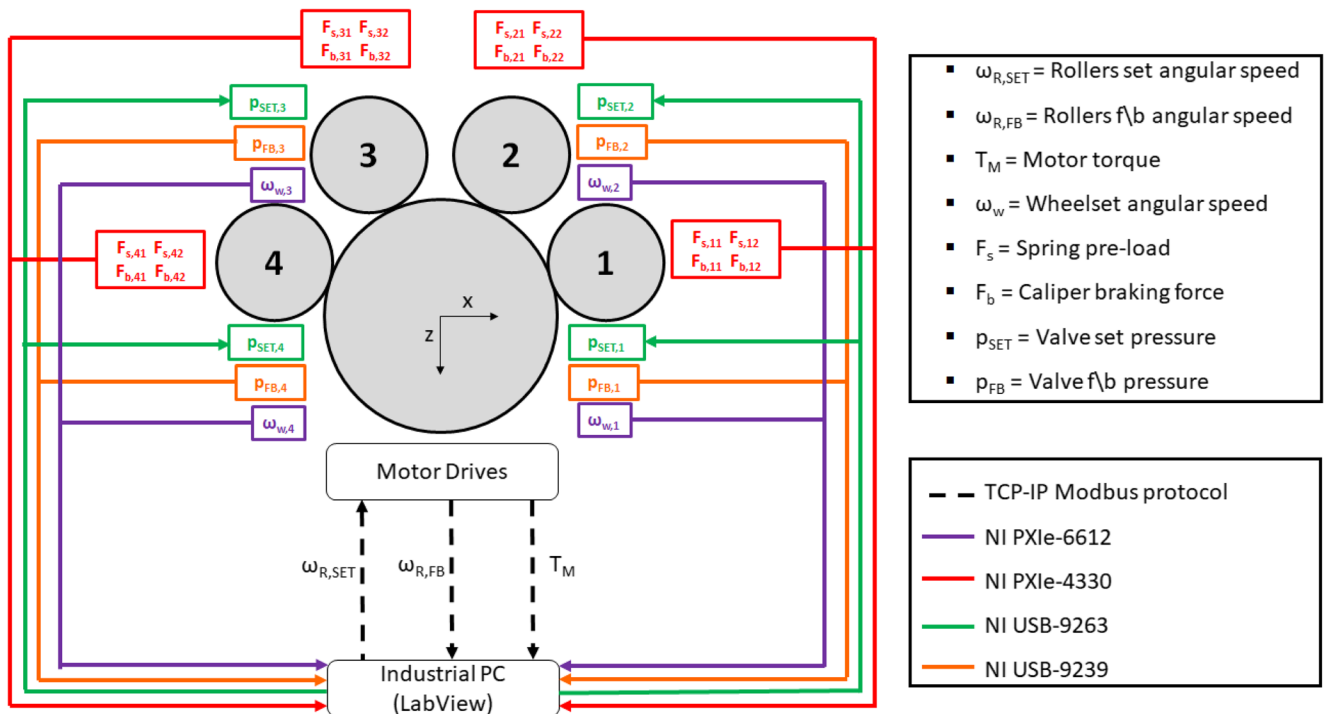


Fig. 7 Schematic view of the control and data acquisition strategy



Table 2 Instrumentation installed on the PoliTo multi-axle roller rig

Instrumentation	Quantity
Measuring instruments	
Encoder ELAP	4
REM470–1024-8/24-R-10-PP2	(One encoder per wheelset)
Load Button Cell	8
FUTEK LLB 400 FSH 00877	(One cell per axle-box)
S-Beam Load Cell	8
FUTEK LSB 302 FSH 02089	(One cell per brake caliper)
Electro-Pneumatic Regulator	4
SMC ITV0050 - 3BS	(One valve per wheelset)
Acquisition devices	
NI PXIe-8330	1 x Industrial controller
NI PXIe-1050	1 x Industrial chassis
NI PXIe-4330	2 x 8 Ch. (Load Cells)
NI PXIe-6612	1 x 8 Counters (Encoders)
NI USB-9239	1 x 4 Analog Input Ch. (F/b Pressure)
NI USB-9263	1 x 4 Analog Output Ch. (Set Pressure)

the range 0 ÷ 10 V using the voltage output module NI USB-9263 managed by the industrial PC. The regulators generate a feedback pressure signal in the range 1 ÷ 5 V, which is acquired by the voltage input module NI USB-9239 also managed by the industrial PC. The resolution of the regulators is about 50 mbar. Each roller is powered by a magnet synchronous AC brushless motor controlled in servo mode thanks to digital inverters. The speed of the rollers and the torque produced by the motor can be acquired from the drives in the LabView software environment installed on the industrial PC by means of the TCP/IP Modbus protocol. The same industrial PC and the same LabView VI are used to acquire the signals of the encoders, of the load cells and of the f/b pressure of the pneumatic valves. At the same time, the software can control the set pressure of all the four pneumatic valves. In this way it is possible to precisely control the wheel-roller creepage independently for each wheelset. Furthermore, it is possible to consider several slip velocities by changing the reference speed of the rollers.

The creep of each axle can be calculated from the angular speeds of the rollers and the wheelset itself as shown in Eq. (1):

$$\xi_i = \frac{\omega_R - \frac{\omega_{w,i}}{\tau}}{\omega_R} \quad (1)$$

where:

- ξ_i is the creep of the i wheelset;
- ω_R is the angular speed of the rollers;
- $\omega_{w,i}$ is the angular speed of the i wheelset;

- τ is the ratio between the roller and the wheel radius. Its theoretical value should be equal to 2, however it was experimentally measured equal to 2.006.

The adhesion coefficient f_i of each wheelset can be calculated according to Eq. (2) if the normal (N_i) and the longitudinal tangential load ($F_{x,i}$) acting on the wheel-roller interface are known.

$$f_i = \frac{F_{x,i}}{N_i} \quad (2)$$

The normal load N_i is the sum of two terms: the load due to the suspension system ($N_{s,i}$), where the subscripts 1 and 2 respectively refer to the right and left side, and the radial component of the weight (Eq. (3)), given by the product of the wheelset mass m and the radial component of the gravitational acceleration. The angle α_i depends on the arrangement of the wheelsets as shown in Fig. 2.

$$N_i = N_{s,i1} + N_{s,i2} + mg\cos\alpha_i = N_{s,i} + mg\cos\alpha_i \quad (3)$$

The mass m of the wheelset was deduced from a multibody Simpack model of the rig and it is equal to 15 kg.

The tangential force can be obtained from an equilibrium of momentum for the wheelset, see Fig. 8 and Eq. (4), if the braking forces acting on the pad are measured:

$$\begin{aligned} F_{x,i} &= \frac{I_{w,yy}\dot{\omega}_{w,i} + (F_{b,i1} + F_{b,i2}) \cdot R_{PAD,i}}{R_w} \\ &= \frac{I_{w,yy}\dot{\omega}_i + F_{b,i} \cdot R_{PAD,i}}{R_w} \end{aligned} \quad (4)$$

where:

- $I_{w,yy}$ is the momentum of inertia of the wheelset along the polar axis, calculated from the Simpack multibody model of the rig (0.025 kg·m²);

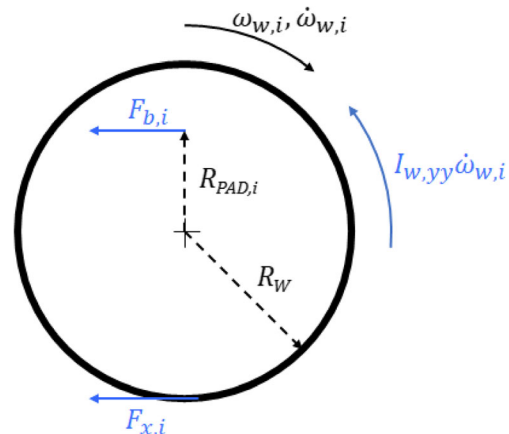


Fig. 8 Equilibrium of momentum of the wheelset

- $\dot{\omega}_{w,i}$ is the angular acceleration of the i wheelset, obtained with a numerical differentiation of the angular speed signal;
- $F_{b,ij}$ is the braking effort measured by the S-Beam Load cells on the right ($j = 1$) or left ($j = 2$) wheel of the i axle;
- R_w is the wheel radius;
- $R_{PAD,i}$ is the brake disc effective radius of the i wheelset, which was experimentally measured as described in the following section.

Once that the adhesion coefficient f_i and the creep ξ_i are calculated it is possible to obtain the adhesion curve for each wheelset.

Experimental Results

This section deals with the laboratory activities carried out during the early stages of the experimental setup of the PoliTo multi-axle roller rig. First, a brief description of the calibration of the load button cells and of the caliper pneumatic valves is shown. Then, attention is drawn to the experimental determination of the effective braking radius of each wheelset. Finally, some adhesion characteristics are presented, obtained by braking either one wheelset at a time or all axes simultaneously.

Calibration of the Load Button Cells

The experimental calibration of the load button cells was performed thanks to the laboratory facility shown in Fig. 9. The load button cell (1) is fastened with bolt joints on the head of a hex-head threaded pin (2), which is tightened on a housing (3). Some known weight masses (4) are placed on a cylindrical element (5). The load is transferred on the button cell by means of a sliding pin (6), which can freely move inside the hex-head threaded pin (2).

Two series of calibration tests were carried out. First, 5 masses of 1 kg each were sequentially applied on the

cylindrical body, and then the system was gradually unloaded. The second series of tests was performed by applying a 10 kg mass and 5 masses of 1 kg each, then unloading the system step by step.

The results of the measuring process showed very good agreement with the calibration data provided by the producer of the sensor, therefore the experimental values were used to carry out the signal acquisition in LabView.

Calibration of the Caliper Pneumatic Valves

The calibration of the solenoid valves led to the determination of both input and output characteristics for all four valves. The experimental procedure, shown in Fig. 10, was performed by imposing a known value of set voltage to the valve in the range $0 \div 10$ V with a step of 0.5 V and by measuring the fb output voltage, both charging and exhausting the pneumatic circuit. The outlet pressure was registered too, by means of a MetalWork 9,000,600 digital pressure switch. The data sheet provided by the producer shows that the input voltage can vary in the range $0 \div 10$ V, while the output voltage is in the range $1 \div 5$ V. Since the pressure can be set in the range $0 \div 9$ bar, the input theoretical characteristic is $p_{SET} = 0,90V_{SET}$, while the output one should be equal to $p_{FB} = 2,25V_{OUT} - 2,24$. Table 3 shows the input and output experimental characteristics for all four pressure regulators: good agreement with the theoretical characteristic was found for the input pressure, so the value of 0,90 bar/V was used in the LabView VI to acquire the four SET pressures. On the other hand, the experimental values were used for the output characteristics.

Determination of the Brake Effective Radius

A very important term to calculate a correct value of the adhesion coefficient with Eqs. (2–4), is the brake effective radius of each caliper. A constant radius of 75 mm could be estimated for all four wheelsets from the CAD model of the rig. However, this quantity has been experimentally measured by characterizing each pair of calipers, installed on the same

Fig. 9 Laboratory device for load button cells calibration: (a) assembly and (b) components

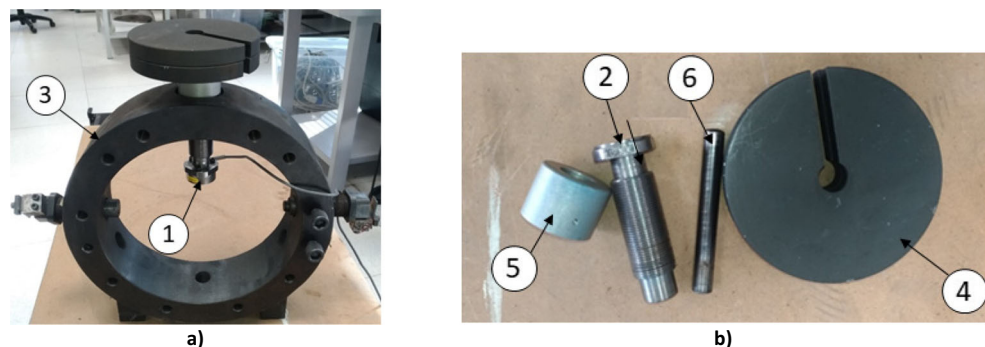
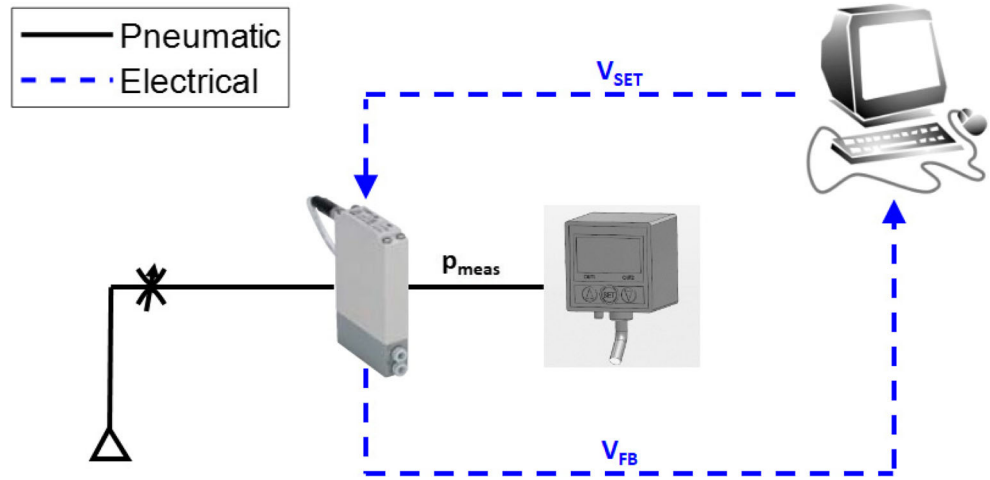


Fig. 10 Solenoid valves: scheme of the calibration procedure



wheelset. The approach is based on the equilibrium of momentum of the rollers when a single wheelset is braked, as shown in Fig. 11.

In fact, when a braking effort is applied on the wheelsets, the torque produced by the motor T_M must balance the total resistant torque of the test bench T_R and the momentum of inertia, as shown in Eq. (5). The total resistant torque is the sum of a constant term, which only depends on the angular speed of the rollers ($T_{R,0}$) and it is due to the rolling resistances of the wheelsets, and a resistant torque due to the braking effort ($T_{R,b}$), which is a function of the caliper pressure p_b of the braked wheelset.

$$T_M = T_R + I_{R,yy}\dot{\omega}_R = T_{R,0}(\omega) + T_{R,b}(p_b) + I_{R,yy}\dot{\omega}_R \quad (5)$$

However, if the pressure is not too high and adhesion is still maintained between the wheel and the roller, a new quasi steady-state condition is reached, and the inertial term can be neglected. With this hypothesis, if the total braking force acting on the pads of the braked wheelset $F_{b,i}$ and the initial resistant torque $T_{R,0}$ are known, the effective braking radius can be calculated according to Eq. (6), where τ is the ratio between the roller and the wheel radius.

$$R_{PAD,i} = \frac{T_M - T_{R,0}(\omega)}{\tau F_{b,i}} \quad (6)$$

Table 3 Solenoid valves: calibration characteristics

No. of The Wheelset	Input Characteristics	Output Characteristics
Wheelset 1	$p_{SET} = 0, 90V_{IN}$	$p_{FB} = 2, 27V_{OUT} - 2, 26$
Wheelset 2	$p_{SET} = 0, 90V_{IN}$	$p_{FB} = 2, 25V_{OUT} - 2, 27$
Wheelset 3	$p_{SET} = 0, 90V_{IN}$	$p_{FB} = 2, 26V_{OUT} - 2, 23$
Wheelset 4	$p_{SET} = 0, 89V_{IN}$	$p_{FB} = 2, 29V_{OUT} - 2, 26$

The experimental determination of the pad radius of each wheelset was carried out by setting the angular speed of the rollers equal to 100 rpm and by registering the initial resistant torque $T_{R,0}$, calculated considering a moving mean with time window of 20 s. Then, the braking pressure of the tested wheelset was set equal to 1 bar and 1,5 bar, and finally the pads were gradually discharged. The effective braking radius was calculated with Eq. (6) after detecting the steady-state condition and measuring the motor torque T_M , smoothed through the same 20 s moving average as the initial resistant torque $T_{R,0}$. The values obtained during this experimental activity are shown in Table 4.

Adhesion Characteristics

After the experimental setup of the rig and the calibration of the sensors, some preliminary tests were performed in order to obtain some adhesion characteristics, simulating a 10-t axle-load on each axle. The tests were performed by setting a pressure ramp from 0 to 6 bar in 12.5 s on the tested wheelsets and stopping the tests when high creep values were detected. During the experimental tests the first wheelset that is in contact with the roller is the fourth one. Fig. 12 shows the adhesion

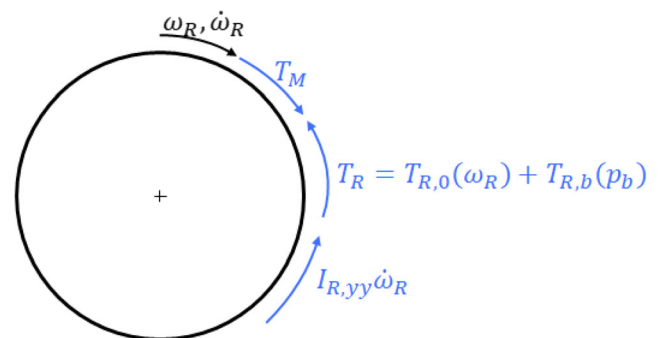


Fig. 11 Equilibrium of momentum of the rollers

Table 4 Resume of the experimental calibration of the wheelset braking radius

Wheelset Number	R _{PAD} (mm) Charging Phase		R _{PAD} (mm) Exhausting Phase		Mean (mm)	St.Dev (mm)	CoV (%)
	$p_b = 1 \text{ bar}$	$p_b = 1,5 \text{ bar}$	$p_b = 1 \text{ bar}$	$p_b = 1,5 \text{ bar}$			
1	79,40	81,42	84,40	82,36	81,90	2,08	2,54%
2	78,55	80,34	82,72	83,54	81,29	2,27	2,79%
3	78,65	81,40	77,45	81,44	79,73	2,01	2,52%
4	77,70	76,91	80,14	81,29	79,01	2,05	2,59%

characteristics acquired by braking one axle at a time, with an angular speed of the rollers equal to 190 rpm (i.e., 30 km/h for a real vehicle). The adhesion characteristics were performed after cleaning the surfaces of rollers and wheels with a soap-based degreaser. Differences among the wheelsets could be due to different adhesion conditions due to the presence of debris generated by the wear process during sliding.

To investigate the repeatability of the results obtained on the rig, two new series of tests were performed with an angular speed of the roller equal to 390 rpm (i.e., 60 km/h for a real vehicle), after cleaning the surfaces with sandpaper. In the first series, all the wheelsets were braked at the same time, whereas in the second series the braking effort was applied on one wheelset at a time. Figure 13 shows good agreement between the two tests, blue colour curve for simultaneous braking and red curve for single wheelset braking, relative to wheelsets 2 and 3. Similar results were obtained for the other axles. Figure 13 shows lower values of adhesion when the braking effort is applied to all the four wheelsets simultaneously with respect to the case when a single axle is braked. This could be due to both an increase in the interface temperature and a contamination of the surfaces related to wear debris produced by the slip.

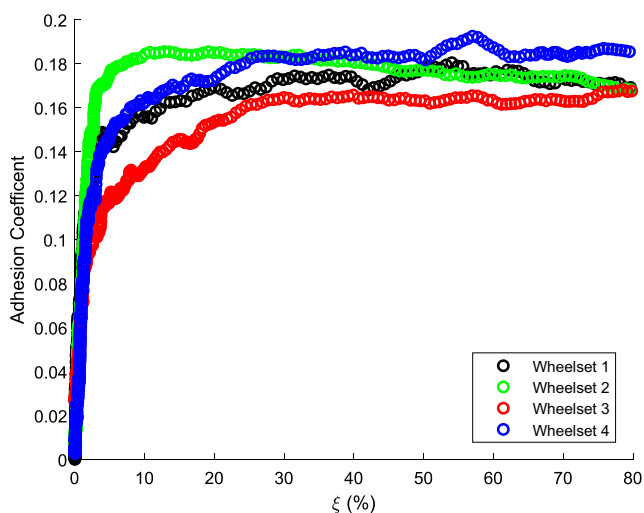


Fig. 12 Adhesion characteristics by braking one axle at a time ($\omega_R = 190 \text{ rpm}$)

The maximum of the adhesion coefficient for the axles differs between Fig. 12 and Fig. 13, due to the loss of adhesion in the first test, where adhesion is reduced by the soap which composes the degreaser. In the second test the soap was removed by the mechanical action of the sandpaper. The preliminary results obtained with the new multi-axle roller rig demonstrate that the bench is suitable for studying the adhesion recovery phenomenon, where it is necessary to evaluate the adhesion conditions considering following wheelsets acting on the same pair of rollers. In particular, the results show that the adhesion condition can be precisely reproduced on all the wheelsets with low variability. This allows to detect very small variations of the adhesion coefficient among the four wheelsets. This characteristic of the test bench is the key to investigate the variation of the friction conditions due to the cleaning effect performed by the leading wheelsets rolling over the contaminated rollers.

Conclusions

This article deals with the experimental setup of an innovative roller rig that can allow the investigation of the adhesion recovery phenomenon due to the cleaning effect of the leading wheelsets of a railway vehicle running along a contaminated track. The literature review shows that an experimental device consisting of more wheels rolling over the same surfaces is needed to study more properly the phenomenon. Current experimental devices do not allow to properly perform this type of tests and the typical limits have been highlighted by several authors. The work demonstrates that this new configuration of roller rig is able to overcome these limitations. The 1:5 scaled multi-axle roller rig is composed of four wheelsets rolling over the same pair of rollers. Several creep conditions can be investigated thanks to a compressed air braking system, which allows an independent control of the braking torque on each wheelset, so that a difference in the peripheral velocities of the wheels and the rollers can be imposed. Many axle-load values can be simulated by means of a suspension system, which can set a desired load on the contact patch of each wheel-roller pair. The signals of several sensors installed on the rig are

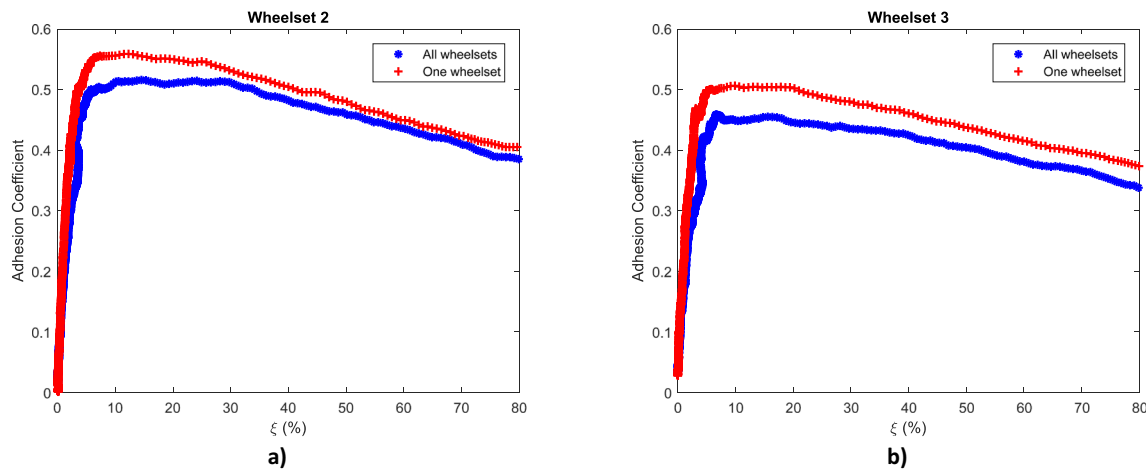


Fig. 13 Adhesion characteristics (a) for wheelset 2 and (b) for wheelset 3 ($\omega_R = 390$ rpm)

acquired to perform the required measurements. The instrumentation underwent an accurate calibration process in order to ensure a good operation of the rig. The paper shows some experimental adhesion characteristics obtained with different surfaces cleaning strategies. The results demonstrate that the test bench allows a good repeatability and that it is able to detect very small variation of the friction coefficient. This characteristic is fundamental in order to evaluate the adhesion recovery phenomenon. In future activities, new adhesion characteristics for several values of axle-load and speed will be acquired. The rig will then be used to perform adhesion recovery investigation and it is expected that the results obtained on the roller rig will contribute to the development of new WSP algorithms.

Compliance with Ethical Standards

Conflict of Interest On behalf of all authors, the corresponding author states that there is no conflict of interest.

References

- Harrison H, McCanney T, Cotter J (2002) Recent developments in coefficient of friction measurements at the rail/wheel interface. *Wear* 253:114–123
- Lewis R, Lewis SR, Zhu Y, Abbasi S, Olofsson U (2013) The modification of a slip resistance meter for measurement of railhead adhesion. *P I Mech Eng F-J Rai* 227(2):196–200
- Olofsson U, Sundvall K (2004) Influence of leaf, humidity and applied lubrication on friction in the wheel-rail contact: pin-on-disc experiments. *P I Mech Eng F-J Rai* 218(3):235–242
- Stolarski TA (1989) Friction in a pin-on-disc configuration. *Mech Mach Theory* 24(5):373–381
- Zhu Y, Olofsson U, Persson K (2012) Investigation of factors influencing wheel-rail adhesion using a mini-traction machine. *Wear* 292-293:218–231
- Galas R, Omasta M, Krupka I, Hartl M (2016) Laboratory investigation of ability of oil-based friction modifiers to control adhesion at wheel-rail interface. *Wear* 368-369:230–238
- Chen H, Ban T, Ishida M, Nakahara T (2008) Experimental investigation of influential factors on adhesion between wheel and rail under wet conditions. *Wear* 265(9–10):1504–1511
- Wang WJ, Liu TF, Wang HY, Liu QY, Zhu MH, Jin XS (2014) Influence of friction modifiers on improving adhesion and surface damage of wheel/rail under low adhesion conditions. *Tribol Int* 75: 16–23
- Lewis SR, Lewis R, Cotter J, Lu X, Eadie DT (2016) A new method for the assessment of traction enhancers and the generation of organic layers in a twin-disc machine. *Wear* 366-367:258–267
- Gallardo-Hernandez EA, Lewis R (2008) Twin disc assessment of wheel/rail adhesion. *Wear* 265(9–10):1309–1316
- Fletcher DI, Lewis S (2013) Creep curve measurement to support Wear and adhesion modelling, using a continuously variable creep twin disc machine. *Wear* 298-299(1):57–65
- Meymand, S, Hosseinipour, M., Ahmadian M. 2015. "The Development of a Roller Rig for Experimental Evaluation of Contact Mechanics for Railway Vehicles. *ASME. ASME/IEEE Joint Rail Conference, 2015 Joint Rail Conference*
- Bosso N, Zampieri N (2014) Experimental and numerical simulation of wheel-rail adhesion and Wear using a scaled roller rig and a real-time contact code. *Shock Vib* 2014
- Bosso N, Zampieri N (2013) Real-time implementation of a traction control algorithm on a scaled roller rig. *Veh Syst Dyn* 51(4):517–541
- Bosso, N., A. Gugliotta, and N. Zampieri. 2014. "Study of adhesion and evaluation of the friction forces using a scaled roller-rig, 5th World Tribology Congress, WTC 2013, Volume 3, 2014, Pages 2640-2643
- Bosso N, Zampieri N (2018) A novel analytical method to calculate wheel-rail tangential forces and validation on a scaled roller-rig. *Advances in Tribology* 2018. <https://doi.org/10.1155/2018/7298236>
- Zhang W, Chen J, Wu X, Jin X (2002) Wheel/rail adhesion and analysis by using full scale roller rig. *Wear* 253(1–2):82–88
- Jaschinski A, Chollet H, Iwnicki S, Wickens A, Von Würzen J (1999) The application of roller rigs to railway vehicle dynamics. *Veh Syst Dyn* 31(5–6):345–392
- Ahn, K., J. Park, and S. Ryew. 2012. "The Construction of a Full-Scale wheel/rail Roller Rig in Korea
- Myamlin, S., J. Kalivoda, and L. Neduzha. 2017. "Testing of Railway Vehicles using Roller Rigs
- Chollet, H. 1998. "Essais en similitude à l'échelle 1r4 de bogies de wagons de la famille Y25
- Iwnicki, S.D. and Shen, Z.Y. 1992. "Collaborative railway roller rig project

23. Jaschinski, A. 1990. "On the application of similarity Laws to a scaled railway bogie model
24. Liu B, Bruni S (2015) Analysis of wheel-roller contact and comparison with the wheel-rail case. *Urban Rail Transit* 1(4):215–226
25. Keylin, A., M. Ahmadian, M. Taheri, and A. Tajaddini. 2012. "Wheel-Rail Contact Characteristics on a Tangent Track Vs a Roller Rig
26. Nakazawa S-I, Hijikata D (2017) Wheel slide protection system by the use of the tangential force in the macro slip area. *Quarterly Report of RTRI (Railway Technical Research Institute)* 58(3): 196–203
27. Barna, G. 2012. "Diagnosis of Wheel Slide Protection Systems for Rail Vehicles
28. Stütze, T., U. Viereck, A. Stribersky, W. Rulka, M. Enning, and D. Abel. 2006. "Creepage Control for use in Wheelslide Protection Systems
29. Kondo, K. 2012. "Anti-Slip Control Technologies for the Railway Vehicle Traction
30. Pichlík, P. Zďenek, j. (2014) Overview of slip control methods used in locomotives. *Transactions on Electrical Engineering* 3(2)
31. Lewis, S. R., R. Lewis, G. Evans, and L. E. Buckley-Johnstone. 2012. "Assessment of railway grease performance using a twin-disc tester
32. Omasta M, Machatka M, Smejkal D, Hartl M, Křupka I (2015) Influence of sanding parameters on adhesion recovery in contaminated wheel-rail contact. *Wear* 322-323:218–225
33. Arias-Cuevas O, Li Z, Lewis R, Gallardo-Hernández EA (2010) Rolling-sliding laboratory tests of friction modifiers in dry and wet wheel-rail contacts. *Wear* 268(3–4):543–551
34. Arias-Cuevas O, Li Z, Lewis R (2011) A laboratory investigation on the influence of the particle size and slip during sanding on the adhesion and Wear in the wheel-rail contact. *Wear* 271(1–2):14–24
35. Li Z, Arias-Cuevas O, Lewis R, Gallardo-Hernández EA (2009) Rolling-sliding laboratory tests of friction modifiers in leaf contaminated wheel-rail contacts. *Tribol Lett* 33(2):97–109
36. Voltr P, Lata M (2015) Transient wheel-rail adhesion characteristics under the cleaning effect of sliding. *Veh Syst Dyn* 53(5):605–618
37. Allotta, B., R. Conti, E. Meli, L. Pugi, and A. Ridolfi. 2014. "Development of a Full-Scale Roller-Rig to Test High Speed Trains Under Degraded Adhesion Conditions
38. Allotta, B., R. Conti, E. Meli, L. Pugi, and A. Ridolfi. 2014. "Study of high-speed train dynamics under degraded adhesion conditions: an innovative HIL architecture for full-scale roller-rigs
39. Bosso N, Gugliotta A, Zampieri N (2015) Strategies to simulate wheel-rail adhesion in degraded conditions using a roller-rig. *Veh Syst Dyn* 53(5):619–634
40. Bosso N, Gugliotta A, Zampieri N (2016) A test rig for multi-wheelset adhesion experiments, vol 110. *Civil-Comp Proceedings*
41. CEN-European Committee for Standardization: EN 15806, railway applications – braking – static brake testing. 2010

Publisher's Note Springer Nature remains neutral with regard to jurisdictional claims in published maps and institutional affiliations.

